Bisphosphonate metal complexes as selective inhibitors of Trypanosoma cruzi farnesyl diphosphate synthase

ARTICLE *in* DALTON TRANSACTIONS · FEBRUARY 2012

Impact Factor: 4.2 · DOI: 10.1039/c2dt12179d · Source: PubMed

13 AUTHORS, INCLUDING:

Mercedes Gonzalez
University of the Republic, Uruguay
234 PUBLICATIONS **4,146** CITATIONS
SEE PROFILE

Hugo Cerecetto
University of the Republic, Uruguay
235 PUBLICATIONS **4,164** CITATIONS
SEE PROFILE

Roberto Docampo
University of Georgia
294 PUBLICATIONS **10,404** CITATIONS
SEE PROFILE

This paper is published as part of a *Dalton Transactions* themed issue entitled:

Application of inorganic chemistry for non-cancer therapeutics

Guest Editor: Katherine J. Franz

Published in issue 21, 2012 of *Dalton Transactions*

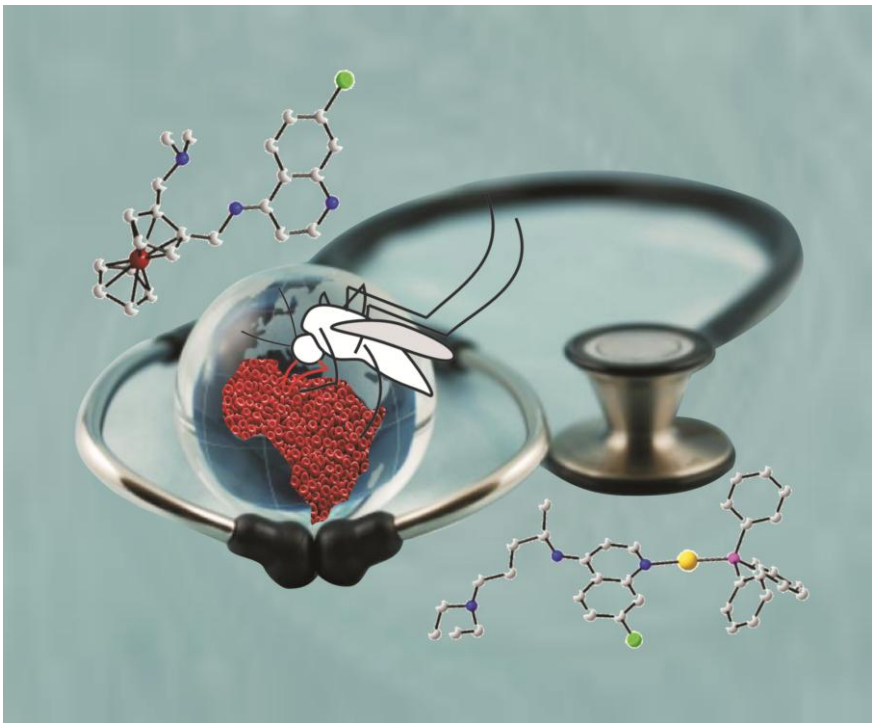

Image reproduced with permission of Christophe Biot

Articles published in this issue include:

Visit the *Dalton Transactions* website for more cutting-edge bioinorganic chemistry research
www.rsc.org/dalton

Dalton Transactions

Dynamic Article Links

Cite this: *Dalton Trans.*, 2012, **41**, 6468

www.rsc.org/dalton

PAPER

Bisphosphonate metal complexes as selective inhibitors of *Trypanosoma cruzi* farnesyl diphosphate synthase†

Bruno Demoro,[a] Francesco Caruso,[b] Miriam Rossi,[c] Diego Benítez,[d] Mercedes González,[d] Hugo Cerecetto,[d] Melina Galizzi,[e] Leena Malayil,[e] Roberto Docampo,[e] Ricardo Faccio,[f] Álvaro W. Mombrú,[f] Dinorah Gambino*[a] and Lucía Otero*[a]

Received 14th November 2011, Accepted 31st December 2011
DOI: 10.1039/c2dt12179d

In the search for a pharmacological answer to treat Chagas disease, eight metal complexes with two bioactive bisphosphonates, alendronate (Ale) and pamidronate (Pam), were described. Complexes of the formula $[M_2^{II}(Ale)_4(H_2O)_2]\cdot 2H_2O$, with M = Cu, Co, Mn, Ni, and $([CuPam]\cdot H_2O)_n$ as well as $[M^{II}(Pam)_2(H_2O)_2]\cdot 3H_2O$, with M = Co, Mn and Ni, were synthesized and fully characterized. Crystal structure of $[Cu_2^{II}(Ale)_4(H_2O)_2]\cdot 2H_2O$, $[Co^{II}(Pam)_2(H_2O)_2]$ and $[Ni^{II}(Pam)_2(H_2O)_2]$ were solved by X-ray single crystal diffraction methods and the structures of $[M_2^{II}(Ale)_4(H_2O)_2]\cdot 2H_2O$ complexes M = Co, Mn and Ni were studied by X-ray powder diffraction methods. All obtained complexes were active against the amastigote form of *Trypanosoma cruzi* (*T. cruzi*), etiological agent of Chagas disease. Most of them were more active than the corresponding free ligands showing no toxicity for mammalian cells. The main mechanism of the antiparasitic action of bisphosphonates, inhibition of parasitic farnesyl diphosphate synthase (*Tc*FPPS), remains in the obtained metal complexes and an increase in the inhibiting enzyme levels was observed upon coordination. Observed enzymatic inhibition was selective for *Tc*FPPS as the metal complexes showed no or little inhibition of human FPPS. Additionally, metal complexation might improve the bioavailability of the complexes through the hindrance of the phosphonate group's ionization at physiological pH and, eventually, through the ability of plasma proteins to work as complex transporters.

1 Introduction

Chagas disease, caused by *Trypanosoma cruzi* (*T. cruzi*), is recognized by the World Health Organization as one of the world's thirteen most neglected tropical illnesses. Despite the efficacy of large-scale programs focused on vector control and quality of transfused blood, Chagas disease is far from being eradicated. In fact, migration flow between Latin America to northern countries at the beginning of the 2000s caused the emergence of imported cases in non-endemic areas such as the United States, Australia, Europe, and Japan.[1,2] Currently, only two drugs are available for the treatment of Chagas disease, nifurtimox and benznidazole, that are poorly tolerated and for which efficacy remains controversial. The main challenge related to this disease is the discovery of new efficient drugs to cure and/or significantly improve the prognosis of the millions of people that are infected.[3]

Information from the complete genome sequence of *T. cruzi* reveals the presence of more than 10 000 protein-coding genes and has allowed the identification of several potential biological targets for drug development.[4–6] Among them, enzymes that are involved in isoprenoid biosynthesis have been identified as drug targets for Chagas chemotherapy. Farnesyl diphosphate synthase (FPPS, 41.2 kDa) is an enzyme involved in the mevalonate pathway, which catalyzes the consecutive condensation of isopentenyl diphosphate with dimethylallyl diphosphate, and with geranyl diphosphate, to form farnesyl diphosphate (FPP). FPP is the substrate for enzymes catalyzing the first step in the biosynthesis of sterols, ubiquinones, dolichols, heme and prenylated proteins, which are important intermediates controlling cell survival and signaling pathways.[7,8]

The most pertinent known inhibitors of this enzyme are the nitrogen containing bisphosphonates (NBP). Several

[a]*Cátedra de Química Inorgánica, DEC, Facultad de Química, Universidad de la República, Gral. Flores 2124, C. C. 1157, 11800 Montevideo, Uruguay. E-mail: dgambino@fq.edu.uy, luotero@fq.edu.uy; Fax: +5982-9241906; Tel: +5982-9249739*
[b]*Istituto Chimica Biomolecolare, CNR, Ple. Aldo Moro, 5, 00185 Rome, Italy*
[c]*Department of Chemistry, Vassar College, Poughkeepsie, New York 12604-0484, USA*
[d]*Grupo de Química Medicinal, Facultad de Química-Facultad de Ciencias, Universidad de la República, Iguá 4225, Montevideo, Uruguay*
[e]*Center for Tropical and Emerging Global Diseases and Department of Cellular Biology, University of Georgia, Athens, USA*
[f]*Centro NanoMat&Cryssmat-lab. DETEMA. Facultad de Química, Universidad de la República, Gral. Flores 2124, C. C. 1157, 11800 Montevideo, Uruguay*

†Electronic supplementary information (ESI) available. CCDC 799811–799813. For ESI and crystallographic data in CIF or other electronic format see DOI: 10.1039/c2dt12179d

bisphosphonates are potent inhibitors of bone resorption and are in clinical use for the treatment and prevention of osteoporosis, Paget's disease, hypercalcemia, tumor bone metastases, and other bone diseases. It has recently become established that the major molecular target of the NBP is the enzyme FPPS within osteoclasts, the cells responsible for bone resorption.[9–11] Crystallographic structures, of some bisphosphonates bound to a variety of FPPS enzymes (from *Staphylococcus aureus*, *Escherichia coli*, *Trypanosoma cruzi*, *Homo sapiens*) have been reported.[12–15] As stated, FPPS belongs to a metabolic route present both in mammalian and parasitic cells. However, the discovery of significant amounts of inorganic polyphosphate, stored in parasite-specific organelles called acidocalcisomes, suggest that bisphosphonates could inhibit the parasite growth in a selective manner.[16,17] Hundreds of bisphosphonate derivatives were found to be potent inhibitors of *T. cruzi* proliferation *in vitro* and *in vivo* without toxicity to the host cells.[18,19] However, some pharmacokinetic drawbacks like poor oral bioavailability (less than 1%) due to the high ionization of phosphonate groups at physiological pH need to be overcome.[5,20] Coordination of bisphosphonates to a metal ion could be a promising strategy to attenuate this disadvantage.

Metal complexation of a bioactive ligand may result in an improvement of the ligand's pharmacological properties. Metal complexes may have dual or even multiple mechanisms of action by combining the biological properties of both the ligand and the metal, leading to synergistic or additive effects. Also, an improvement in the ligand's pharmacokinetics, biodistribution, and biotransformation may be achieved as complex formation could alter the ligand's solubility and lipophilicity and/or restrict the formation of highly charged species by binding of groups that are charged at physiological pH.[21] Even though medicinal inorganic chemistry has mainly placed emphasis on the development of metal-based chemotherapeutics for cancer treatment, some interesting potential metallopharmaceuticals for the treatment of parasitic diseases have been developed.[22–24] Our group has been involved in the coordination of bioactive ligands against Chagas disease with a variety of metal ions. Many of the obtained metal complexes were more active than the free ligands and their mechanisms of action were extensively studied.[25–38] In particular, we had previously developed metal complexes with the bioactive bisphosphonate risedronate. Results demonstrated that the coordination of risedronate to different metal ions improved its antiproliferative effect against *T. cruzi* exhibiting IC_{50} values against the intracellular amastigote form of the parasite in the low micromolar levels. Moreover, this high activity could be correlated to high inhibition of the *T. cruzi* FPP synthase enzyme.[37]

Based on these results, we expand our investigations to other bioactive bisphosphonates: alendronate and pamidronate (Fig. 1). The choice of the metal ions relied on different chemical and biological reasons. As previously explained, we intended to coordinate the bioactive ligands through the highly ionizable bisphosphonate groups to obtain neutral species. Therefore, hard or intermediate M(II) ions, like Cu(II), Mn(II), Ni(II) and Co(II), that could bind to the hard oxygen donor atoms were selected. In addition, selection of these essential metal ions was based on the assumption that endogenous metals may be less toxic than non-essential ones. On the other hand, as Mg(II) ions are necessary for the binding of bisphosphonates to FPPS,[11] metal(II) ions could improve their binding ability, leading to a higher enzymatic inhibition and thus higher antiparasitic activity.

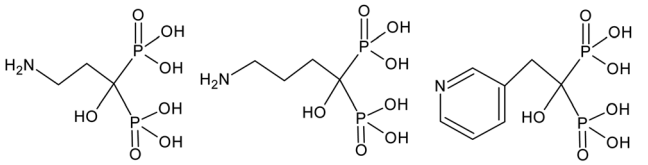

Fig. 1 Chemical structure of selected bisphosphonates (acid forms): pamidronate (3-amino-1-hydroxypropane-1,1-diylphosphonic acid), alendronate (4-amino-1-hydroxybutane-1,1-diylphosphonic acid), risedronate (1-hydroxy-2-(pyridin-3-yl)ethane-1,1-diylphosphonic acid).

In this work, we present the synthesis and characterization of eight novel bisphosphonate metal complexes. Their *in vitro* antiproliferative effect on *T. cruzi* epimastigotes and amastigotes and their ability for inhibiting both *Trypanosoma cruzi* and human FPPS (*Tc*FPPS and *Hs*FPPS) are evaluated. In addition, the complexes' interaction with albumin is studied, since it could provide a way to transport them *in vivo* in the blood. Biological results are compared to those obtained for previously reported risedronate (Fig. 1) complexes.

2 Experimental

2.1 Materials

Sodium alendronate trihydrate (4-amino-1-hydroxybutane-1,1-diylphosphonic acid sodium salt, NaAle), and sodium pamidronate (3-amino-1-hydroxypropane-1,1-diylphosphonic acid sodium salt, NaPam), as well as reagent grade chemicals and solvents were purchased from commercial sources and used without further purification.

2.2 Synthesis procedures

Syntheses of $[M^{II}_2(Ale)_4(H_2O)_2]\cdot 2H_2O$, with M = Mn, Co, Ni, Cu. NaAle (50 mg, 0.15 mmol) was dissolved in 5 mL of water and the solution's pH value was adjusted to 2–3 by addition of HCl solution. The corresponding amount (0.075 mmol) of $MCl_2\cdot xH_2O$ (with M = Mn, Co, Ni and Cu and x = 4, 6, 6, 2, respectively) was added. After 24 h at room temperature, a solid was filtered off.

$[Cu_2(Ale)_4(H_2O)_2]\cdot 2H_2O$ (yield: 31 mg, 37%) was obtained as sky light blue prismatic crystals. Found: C, 16.0; H, 4.3; N, 4.5; calc. for $C_{16}H_{52}N_4O_{32}P_8Cu_2$: C, 16.2; H, 4.4; N, 4.7.

$[Co_2(Ale)_4(H_2O)_2]\cdot 2H_2O$ (yield: 38 mg, 46%) was obtained as a pink microcrystalline solid. Found: C, 16.2; H, 4.6; N, 4.9; calc. for $C_{16}H_{52}N_4O_{32}P_8Co_2$: C, 16.3; H, 4.4; N, 4.8.

$[Ni_2(Ale)_4(H_2O)_2]\cdot 2H_2O$ (yield: 33 mg, 40%) was obtained as a greenish microcrystalline solid. Found: C, 16.2; H, 4.4; N, 5.0; calc. for $C_{16}H_{52}N_4O_{32}P_8Ni_2$: C, 16.3; H, 4.4; N, 4.8.

$[Mn_2(Ale)_4(H_2O)_2]\cdot 2H_2O$ (yield: 41 mg, 49%) was obtained as a pink microcrystalline solid. Found: C, 16.3; H, 4.3; N, 4.6; calc. for $C_{16}H_{52}N_4O_{32}P_8Mn_2$: C, 16.4; H, 4.4; N, 4.8.

Table 1 Crystal data and structure refinement for single crystal complexes

Name	$[Cu_2(Ale)_4(H_2O)_2]\cdot 2H_2O$	$[Co(Pam)_2(H_2O)_2]$	$[Ni(Pam)_2(H_2O)_2]$
Empirical formula	$C_{16}H_{52}Cu_2N_4O_{30}P_8\cdot 2H_2O$	$C_6H_{24}CoN_2O_{16}P_4$	$C_6H_{24}N_2NiO_{16}P_4$
Shape, color	Block, colorless	Needle, pink	Square, pink
Crystal system	Monoclinic	Monoclinic	Monoclinic
Space group	$P2_1/c$	$P2_1/n$	$P2_1/n$
Temperature (K)	125(2)	125(2)	125(2)
Wavelength (Å)	0.71073	0.71073	0.71073
a (Å)	12.5988(14)	7.350(6)	7.338(2)
b (Å)	13.3968(15)	10.851(9)	10.831(4)
c (Å)	12.5122(14)	10.908(9)	10.907(4)
β (°)	110.935(1)	94.407(11)	94.356(4)
Volume (Å^3)	1972.4(4)	867.3(13)	864.4(5)
Z, density (mg mm^{-3})	2, 1.999	2, 2.156	2, 2.163
Absorption coefficient	1.518	1.451	1.586
Crystal size (mm)	0.12 × 0.06 × 0.06	0.21 × 0.07 × 0.04	0.15 × 0.14 × 0.05
θ range data collection	1.73, 30.42	2.65, 22.21	2.65, 28.28
Limiting indices	−17, 17/−18, 18/−17, 17	−7, 7/−11, 11/−11, 11	−9, 9/−14, 14/−14, 14
Data collected/unique/R_{int}	0.0615	6487/1097/0.0669	11 028/2150/0.0446
Max, min. transmission	0.91/0.84	0.94/0.75	0.92/0.80
Refinement method	F^2	F^2	F^2
Refined data/parameters	4218/288	887/113	1773/118
Goodness-of-fit on F^2	1.023	1.190	1.212
Final R,[a] Rw(all) [$I > 2\sigma(I)$]	0.0462, 0.1239	0.0399, 0.1096	0.0397, 0.1143

[a] $R_1 = \Sigma||F_o| - |F_c||/\Sigma|F_o|$, w$R_2 = [\Sigma w(|F_o|^2 - |F_c|^2)^2/\Sigma w(|F_o|^2)^2]^{1/2}$.

Syntheses of $([Cu^{II}(Pam)]\cdot H_2O)_n$ and $[M^{II}(Pam)_2(H_2O)_2]\cdot 3H_2O$, with M = Mn, Co, Ni. Na_2Pam (50 mg, 0.18 mmol) was dissolved in 5 mL of water and the solution's pH value was adjusted to 2 by addition of HCl solution. The corresponding amount (0.090 mmol) of $MCl_2\cdot xH_2O$ (with M = Mn, Co, Ni and Cu and x = 4, 6, 6, 2, respectively) was added. After 24 h at room temperature, a solid was filtered off.

$([Cu^{II}(Pam)]\cdot H_2O)_n$ (yield: 26 mg, 46%) was obtained as sky blue prismatic crystals. Found: C, 11.4; H, 3.4; N, 4.7; calc. for $C_3H_{11}NO_8P_2Cu$: C, 11.5; H, 3.5; N, 4.5.

$[Co(Pam)_2(H_2O)_2]\cdot 3H_2O$ (yield: 28 mg, 55%) was obtained as a pink microcrystalline solid. Found: C, 11.5; H, 4,7; N, 4.7; H_2O 8.5; calc. for $C_6H_{30}N_2O_{19}P_4Co$: C, 11.7; H, 4.9; N, 4.5; H_2O, 8.8.

$[Ni(Pam)_2(H_2O)_2]\cdot 3H_2O$ (yield: 21 mg, 41%) was obtained as a greenish microcrystalline solid. Found: C, 11.5; H, 4.8; N, 4.5; H_2O 9.2; calc. for $C_6H_{30}N_2O_{19}P_4Ni$: C, 11.7; H, 4.9; N, 4.5; H_2O, 8.8.

$[Mn(Pam)_2(H_2O)_2]\cdot 3H_2O$ (yield: 23 mg, 46%) was obtained as a white microcrystalline solid. Found: C, 11.6; H, 5.0; N, 4.7; H_2O, 8.5; calc. for $C_6H_{30}N_2O_{19}P_4Mn$: C, 11.7; H, 4.9; N, 4.6; H_2O 8.8.

2.3 Physicochemical characterization

C, H and N analyses were performed with a Carlo Erba Model EA1108 elemental analyzer. FTIR spectra (4000–200 cm^{-1}) of the complexes and the free ligands were measured as KBr pellets with a Bomen FTIR model M102 instrument. Thermogravimetric measurements (TGA) were done on a Shimadzu TGA 50 thermobalance, with a platinum cell, working under flowing nitrogen (50 mL min^{-1}) and at a heating rate of 0.5 °C min^{-1} (RT–80 °C range) and 1.0 °C min^{-1} (80–350 °C range).

2.4 Crystallographic study

X-ray crystal diffraction. Suitable crystals for X-ray diffraction data were obtained from the synthesis solutions. Data of the $[Cu_2(Ale)_4(H_2O)_2]\cdot 2H_2O$, $([Cu(Pam)]\cdot H_2O)_n$, $[Co(Pam)_2(H_2O)_2]$ and $[Ni(Pam)_2(H_2O)_2]$, were collected at low temperature by using graphite monochromated MoKα radiation in a Bruker SMART APEX II CCD X-ray diffractometer. Crystal parameters of the obtained CuPam complex correspond to those previously reported for $([Cu^{II}(Pam)]\cdot H_2O)_n$.[39] The Co complex gave a limited number of useful reflections and so some C atoms were refined isotropically. Structure resolution and refinement were performed using ShelX.[40] Details are included in Table 1.

X-ray powder diffraction. X-ray powder diffraction data were collected for all the polycrystalline samples using a Rigaku ULTIMA IV, 285 mm radius, powder diffractometer operating in Bragg Brentano geometry. CuKα radiation (λ = 1.5418 Å) monochromatized with a diffracted beam bent germanium crystal was used to collect data over the 2–70° 2θ range in steps of 0.02° using a scintillation detector. Fixed slits of 1/3° were used for data collection to prevent beam spillage outside the 2 cm long sample (along the beampath) at low angles. Peak positions were extracted from the data using the software POWDERX[41] and peak indexing and unit cell determination was performed with the software DICVOL04,[42] in order to determine the unit cell and space group symmetry of the crystalline samples.

2.5 *In vitro* activity on *T. cruzi* epimastigotes

Handling of live *T. cruzi* was done according to established guidelines.[43] The epimastigote form of the parasite Tulahuen 2 strain was grown at 28 °C in an axenic medium (Brain–Heart Infusion (BHI)-Tryptose Agar), complemented with 5% fetal

calf serum. Cells from a 5 days-old culture were inoculated into 50 mL of fresh culture medium to give an initial concentration of 1×10^6 cells mL^{-1}. Cell growth was followed by daily measuring the absorbance A of the culture at 600 nm for 5 days. Before inoculation, the media was supplemented with a 50 μM dose of the alendronate as well as pamidronate metal compounds by addition of an appropriate aliquot of a stock buffer phosphate solution pH 7.2, 5.5 mM glucose.[37] The compound's ability to inhibit the growth of the parasite was evaluated, in triplicate, in comparison to the control. The control was run in the absence of any drug. Metal salts showed no effect on parasite growth. The percentage of growth inhibition (PGI) was calculated as follows: $\% = \{1-[(A_p - A_{0p})/(A_c - A_{0c})]\} \times 100$, where $A_p = A_{600}$ of the culture containing the drug at day 5; $A_{0p} = A_{600}$ of the culture containing the drug just after addition of the inoculum (day 0); $A_c = A_{600}$ of the culture in the absence of any drug (control) at day 5; $A_{0c} = A_{600}$ in the absence of the drug at day 0. Reported values are the mean of three independent experiments with a SD less than 10%.

2.6 Drug screening assays *in Vero* cells and *T. cruzi* intracellular amastigotes

Gamma-irradiated (2000 Rads) Vero cells (3.4×10^4 cells per well) were seeded in 96 well plates (black, clear bottom plates from Greiner Bio-One) in 100 μL RPMI media (Sigma) with 10% FBS. Plates were incubated overnight at 35 °C and 7% CO_2. After overnight incubation, Vero cells were challenged with 3.4×10^5 trypomastigotes per well (CL strain overexpressing a tdTomato red fluorescent protein)[44] in 50 μL volume and incubated for 5 h at 35 °C and 7% CO_2. After infection, wells were washed once with Hanks solution (150 μL per well) to eliminate any extracellular parasites and compounds were added in serial dilutions in RPMI media in 150 μL volumes. Each dilution was tested in quadruplicate. Each plate also contained controls with host cells and no parasites (for background check), controls with two representative drug dilutions and no parasites (for cytotoxicity assays), and controls with parasites and no drugs (positive control). For each plate, benznidazole was also used as a positive control at 3.5 and 1.5 μM. After drug addition, plates were incubated at 35 °C and 7% CO_2. At day 3 post-infection, plates were assayed for fluorescence. IC_{50} values were determined by non-linear regression analysis using SigmaPlot.

2.7 FPPS inhibition assay

*Hs*FPPS was expressed and purified as previously described.[45] *Tc*FPPS was obtained as described before.[7] The FPPS inhibition radiometric assay was performed essentially as previously reported.[46] Briefly, 150 μL of assay buffer (10 mM Hepes (4-(2-hydroxyethyl)-1-piperazineethanesulfonic acid), pH 7.4, 5 mM $MgCl_2$, 2 mM dithiothreitol, 4.7 μM [4-^{14}C]IPP (isopentenyl diphosphate) (10 μCi μmol^{-1})) and 55 μM DMAPP (dimethylallyl pyrophosphate) were prewarmed to 37 °C. The assay was initiated by the addition of recombinant protein (10–20 ng). The assay was allowed to proceed for 30 min at 37 °C and was quenched by the addition of 6 M HCl (10 μL). The reaction mixtures were made alkaline with 6.0 M NaOH (15 μL), diluted in water (0.7 mL), and extracted with hexane (1 mL). The hexane solution was washed with water and 500 μL of the hexane fraction was transferred to a scintillation vial for counting. One unit of enzyme activity was defined as the activity required to incorporate 1 nmol of [4-^{14}C]IPP into [14-^{14}C]FPP (FPP) in 1 min. IC_{50} values were determined by non-linear regression analysis using SigmaPlot.[7,47] 10 μL of several dilutions of the complexes were used for the inhibition assay. Positive (no inhibitor, only enzyme) and negative controls (no inhibitor and no enzyme) for each experiment were performed.

2.8 Interaction with proteins

The interaction of the complexes with albumin (BSA) was performed according to previously reported methods.[48] BSA (500 μM) and metal complexes in a 1 : 1 molar relationship were incubated at 37 °C in 100 mM phosphate buffer, pH 7.4, 0.15 M NaCl, for 48 h. BSA (including BSA with bound metal complex) was separated from the other components of the solution (unbound metal complex) based in their significantly different molecular weights. For this purpose the incubated solutions were ultrafiltrated using Centrikon tubes (10 000 Da cut-off). A control assay was performed without the addition of BSA to discard filter adsorption of the complexes. The amount of unbound complex in the filtrate was quantified by atomic absorption spectrometry using a Perkin Elmer 5000 spectrometer.

3 Results and discussion

3.1 Chemistry

Four metal complexes using alendronate (Fig. 1), and four others using pamidronate (Fig. 1) as ligands have been synthesized and fully characterized. $[M_2^{II}(Ale)_4(H_2O)_2]\cdot 2H_2O$, with M = Cu, Co, Mn, Ni, and $([CuPam]\cdot H_2O)_n$ as well as $[M^{II}(Pam)_2(H_2O)_2]\cdot 3H_2O$ with M = Co, Mn and Ni were obtained in good yields and high purities by direct synthesis in aqueous solution at room temperature. It should be noted that microcrystalline powder of MPam complexes obtained from the synthesis solution present a different number of crystallization water molecules than crystals useful for X-ray single crystal diffraction for structure solution. However, analytical data, including thermogravimetric analysis results confirmed the proposed formula for all obtained complexes.

3.2 Infrared studies

Infrared spectra of pamidronate and alendronate ligands as well as the corresponding complexes were analyzed in order to assign significant infrared vibration bands useful for determining the bisphosphonate ligands mode of coordination. However, extensive overlapping of absorption bands complicated the assignment of the IR spectra.

It is relevant to notice that infrared spectra of $[M_2^{II}(Ale)_4(H_2O)_2]$ compounds with M = Cu, Co, Mn, Ni are almost identical, which is in accordance with the fact that all alendronate complexes were isostructural (see X-ray powder studies below). For $[M^{II}(Pam)_2(H_2O)_2]$, where M = Co, Mn, Ni,

Table 2 Relevant bond distances and angles around the metal ion in $[Cu^{II}_2(Ale)_4(H_2O)_2]\cdot 2H_2O$

Angle (°)		Distance (Å)	
O9–Cu–O20/O21(#1)–Cu–O4	174.6(1)/176.5(1)	Cu–O4	2.023(2)
O99–Cu–O58	178.2(1)	Cu–O9	1.941(2)
O20–Cu–O21(#1)/O(9) –Cu–O(4)	98.7(1)/91.3(1)	Cu–O20	1.946(2)
O20–Cu–O4/O9–Cu–O99	83.5(1)/88.8(1)	Cu–O21(#1)	2.002(2)
O20–Cu–O99/O21(#1) –Cu–O99	90.0(1)/88.7(1)	Cu–O58	2.405(2)
O4–Cu–O99/O9–Cu–O58	94.0(1)/91.5(1)	Cu–O99	2.289(3)
O20–Cu–O58/O21(#1) –Cu–O58	89.9(1)/89.5(1)		
O4–Cu–O58/O(9) –Cu–O(21)#1	87.8(1)/86.5(1)		

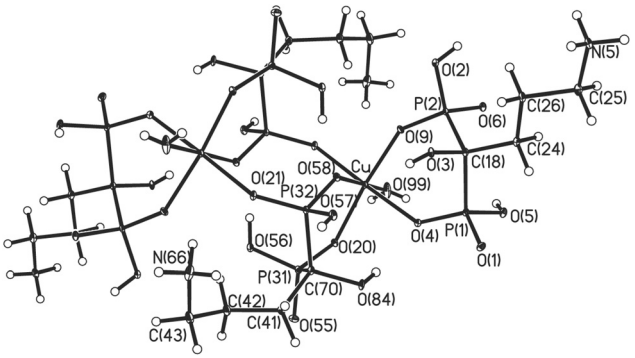

Fig. 2 Molecular structure of $[Cu^{II}_2(Ale)_4(H_2O)_2]\cdot 2H_2O$ showing ellipsoids at 50% probability level.

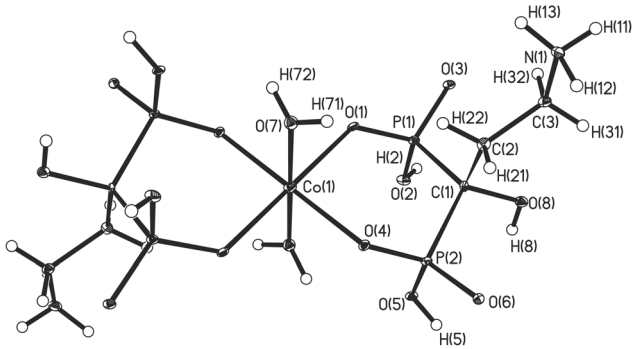

Fig. 3 Molecular structure of $[Co(Pam)_2(H_2O)_2]$.

a quite similar spectral behavior is also observed showing clear evidence of similar structural features. As expected, the IR spectrum of the $([Cu^{II}(Pam)]\cdot H_2O)_n$ chain is different to those of the other pamidronate complexes.

In the 1100–1250 cm^{-1} region, POO– stretching bands are observed.[49] These bands are shifted to lower frequencies in all the obtained metal complexes. This is consistent with the bidentate coordination of pamidronate and alendronate ligands through the phosphonate groups in all the monomeric metal complexes.[37] The bridging mode of coordination of the bisphosphonate ligands in the CuPam chain and in the alendronate complexes was evidenced as an important decrease or disappearance of one of the stretching POO– bands.

3.3 Crystal structures

Crystal structure of $[Cu^{II}_2(Ale)_4(H_2O)_2]\cdot 2H_2O$. Relevant intra-molecular bond distances and angles around the metal center are shown in Table 2. Fig. 2 depicts a drawing of the molecule including displacement ellipsoids at the 50% probability level.

The X-ray diffraction data show two equivalent Cu atoms in the complex, they are related through the crystallographic inversion center at the vertices of the cell and so half a molecule forms the independent crystallographic unit. Thus, the Cu–alendronate species is a dinuclear complex whose central 8-membered ring is made by 2 Cu, 2 P and 4 O atoms. The metal is surrounded by 6 O atoms, two of them from a chelating bisphosphonate, 3 other O(phosphonato) are bridging the other Cu center (forming a Cu–O–P–O–Cu arrangement) and an aqua donor completes the octahedral coordination sphere. The equatorial oxygen atoms (O4, O9, O20 and O21) are almost coplanar with the metal center and their Cu–O bond distance range is 1.941(2)–2.023(2) Å, whereas the axial Cu–O bonds are elongated [Cu–O(aqua) = 2.289(3) Å, Cu–O(58) = 2.405(3) Å] in agreement with the Jahn–Teller effect characteristic of ions with a d^9 electronic configuration.

All coordinated alendronate ligands are monoanionic. All phosphonates are not equivalent, half of them chelate the metal and the other half are bridging entities. All of them contain a P–OH moiety and show two bonding oxygen donors to the metal. The chelating phosphonates form a *cis* binding and have a P═O moiety. Since the bridging phosphonates define the Cu–O–P–O–Cu arrangement their P═O moiety is missing. In addition, the aqua ligand is *trans* to the bridging phosphonate, while there is a NH_3^+ terminal group. The P–OH moiety does not interact with the metal; rather it participates in H bonding. As a matter of fact, there is an extensive network of intra and intermolecular hydrogen bonds between the molecular units, which includes both coordinated (aqua) and lattice (hydrate) water species, as shown in Table S1 (ESI†).

Crystal structure of $[Co^{II}(Pam)_2(H_2O)_2]$ and $[Ni^{II}(Pam)_2(H_2O)_2]$. Both pamidronate metal compounds show very similar coordination spheres (Fig. 3 and 4). Selected bond distances and angles are presented in Tables 3 and 4. The metal resides on an inversion center so that these complexes are centrosymmetric. In both Co– and Ni–pamidronate complexes, two ligands chelate the metal center through two oxygens being both pamidronates in *trans* positions; two aqua molecules complete the octahedral coordination sphere. Both coordinating phosphonate oxygen atoms are deprotonated while the amine nitrogen is protonated resulting in a −1 net charge for each pamidronate ligand.

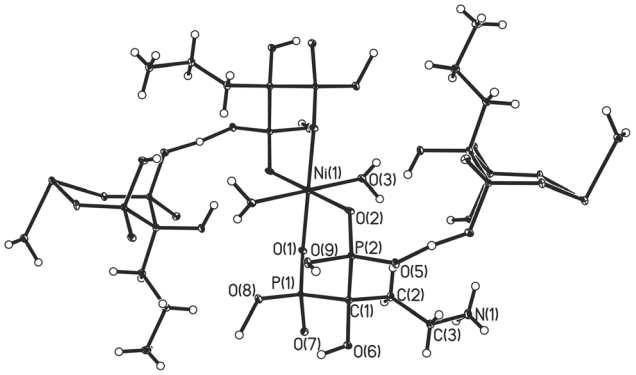

Fig. 4 Molecular structure of $[Ni(Pam)_2(H_2O)_2]$.

In the Ni complex the pamidronate chelate has bond distances Ni–O1 and Ni–O2 that are significantly different [2.029(2) Å and is 2.110(2) Å, respectively]; the Ni–O(aqua) bond length is intermediate [Ni–O3 = 2.082(2) Å]. In the Co–pamidronate complex the ligand asymmetry is confirmed [Co–O4 = 2.056(4), Co–O1 = 2.128(4)] but the Co–O(aqua) [Co–O7 = 2.133(5) Å] is equal to the longer Co–O(pamidronate). The bite angles in Co and Ni pamidronate complexes are similar as well [92.9(1)° and 93.26(8)°, respectively]; they are slightly wider than those in the Cu–alendronate species [91.3(1)°]. On the whole, the Co coordination sphere is expanded compared to the Ni one. In both complexes there is an extensive network of intra and intermolecular hydrogen bonds (Tables S2 and S3, ESI†).

When comparing with the literature, the Ni and Co complexes have similar coordination geometry to another metal–bisphosphonato species, $[Ni^{II}(risedronate)_2(H_2O)_2]$.[37]

3.4 X-ray powder diffraction studies of $[M^{II}_2(Ale)_4(H_2O)_2]\cdot 2H_2O$ complexes

Bisphosphonic acids are good chelators for divalent cations (M),[50] one example is the case of alendronate. According to the CCSD (Cambridge Crystallographic Structure Data Base), just a few coordination compounds have been reported. Among them we can distinguish two kinds of structures: bis(μ_2-4-ammonio-1-hydroxbutylidene-1,1-diphosphonato)-diaqua-bis(4-ammonio-1-hydroxybutylidene-1,1-diphosphonato)-di-M_a(II)dihydrate (M_a = Co and Zn), and catena-(4-amino-1-hydroxybutylidene-1,1-bisphosphonite-M_b monohydrate) (M_b = Mn and Cd).[50–52]

Table 5 Refined cell parameters for all the compounds in the $P2_1/c$ space group

Structure	a (Å)	b (Å)	c (Å)	β (°)
CuAle (Rietveld)	12.617(1)	13.474(1)	12.533(1)	111.01(1)
CuAle	12.623(3)	13.467(2)	12.529(2)	110.95(1)
MnAle	12.698(2)	13.691(4)	12.446(3)	109.81(2)
CoAle	12.579(3)	13.601(3)	12.429(2)	109.92(1)
NiAle	12.509(1)	13.537(2)	12.509(2)	109.542(2)

On these bases, other M–alendronate coordination compounds could crystallize in one of these two general structures. According to the measured data, all the prepared compounds, present very similar X-ray powder diffraction patterns. After the peak indexing routine, involving twenty peaks in all the cases, all the structures presented the monoclinic $P2_1/c$ space group; with very similar structural parameters to the analogue $C_{16}H_{52}Co_2N_4O_{30}P_8\cdot 2H_2O$ (see Table 5 for details). This compound presents cell parameters a = 12.556(8) Å, b = 13.501(5) Å, c = 12.423(5) Å, α = 90.00°, β = 109.92(8)°, γ = 90.00°. It is a dinuclear compound, with a pseudo-octahedral metal environment, established by the alendronate ligand and completed by two water molecules. In this structure, both phosphonic acid groups are deprotonated, providing a bidentate dianionic group, where each phosphonate is in the form –P═O(O^-)(OH). According to this, the ligand adopts a simple chelate and chelate bridging coordination disposition. There are important intra- and inter-hydrogen bonds, in one hand between C–OH–HO–P groups where both are part of the same bridging ligand and on the other hand between C–OH–(Co)O–P groups from bridging to terminal ligands. Further intramolecular hydrogen bonds, of type NH_3^+–(Co)O–P from bridging to terminal ligands are also present.[50]

Performed studies confirm, on one hand, the synthesis of the $C_{16}H_{52}Co_2N_4O_{30}P_8\cdot 2H_2O$ compound. On the other hand, this is a demonstration that new isostructural $C_{16}H_{52}M_2N_4O_{30}P_8\cdot 2H_2O$ compounds have been prepared.

Further confirmation could be obtained from a full pattern profile fitting, using the Rietveld method,[53] by means of the

Table 3 Relevant bond distances and angles in the coordination sphere of $[Co^{II}(Pam)_2(H_2O)_2]$

Angle (°)		Distance (Å)	
O4–Co–O7/O4–Co–O7′	87.1(2)/92.9(2)	Co–O7/Co–O7′	2.133(5)/2.133(5)
O7–Co–O1/O7–Co–O1′	90.0(2)/90.0(2)	Co–O1/Co–O1′	2.128(4)/2.128(4)
O1–Co–O4/O1–Co–O4′	87.1(2)/92.9(2)	Co–O4/Co–O4′	2.056(4)/2.056(4)
O1–Co–O1′/O4–Co–O4′/O7–Co–O7′	180/180/180		

Table 4 Relevant bond distances and angles in the coordination sphere of $[Ni^{II}(Pam)_2(H_2O)_2]$

Angle (°)		Distance (Å)	
O1–Ni–O2′/O1–Ni–O2	86.74(8)/93.26(9)	Ni1–O3/Ni–O3′	2.082(2)/2.082(2)
O1–Ni–O3′/O1–Ni–O3	88.03(9)/91.97(9)	Ni1–O2/Ni–O2′	2.110(2)/2.110(2)
O2–Ni–O3/O2–Ni–O3′	89.98(9)/90.02(9)	Ni1–O1/Ni–O1′	2.029(2)/2.029(2)
O1–Ni–O1′/O2–Ni–O2′/O3–Ni–O3′	180/180/180		

Table 6 Results of biological assays performed on the obtained metal bisphosphonate complexes

Compound	$PGI_{50\mu M}$ (%)[a] (epimastigotes)	IC_{50} (μM)[b] (amastigotes)	IC_{50} (μM)[c] (*Tc*FPPS)	IC_{50} (μM)[d] (*Hs*FPPS)
Pamidronate	0	38.8 ± 5.0	1.340 ± 0.013	>10
$([Cu^{II}(Pam)]\cdot H_2O)_n$	32	11.18 ± 3.3	0.095 ± 0.020	>10
$[Co^{II}(Pam)_2(H_2O)_2]$	26	11.18 ± 3.3	0.215 ± 0.049	>10
$[Ni^{II}(Pam)_2(H_2O)_2]$	24	12.46 ± 2.8	0.328 ± 0.080	>10
$[Mn^{II}(Pam)_2(H_2O)_2]$	15	17.0 ± 0.4	0.161 ± 0.089	>10
Alendronate	0	38.3 ± 2.3	4.40 ± 0.48	>10
$[Cu^{II}{}_2(Ale)_4(H_2O)_2]$	10	13.9 ± 5.7	0.717 ± 0.137	>10
$[Co^{II}{}_2(Ale)_4(H_2O)_2]$	24	26.5 ± 9.0	>50	>10
$[Ni^{II}{}_2(Ale)_4(H_2O)_2]$	19	19.9 ± 7.7	0.167 ± 0.020	>10
$[Mn^{II}{}_2(Ale)_4(H_2O)_2]$	1	14.3 ± 6.2	0.128 ± 0.031	>10
Risedronate	19[e]	55 ± 5[e]	0.0270 ± 0.009	0.030 ± 0.026
$[Cu^{II}(Ris)_2]$	16[e]	23 ± 7[e]	0.0260 ± 0.0048	0.479 ± 0.116
$[Co^{II}(Ris)_2]$	32[e]	>50[e]	>0.1	>0.1
$[Ni^{II}(Ris)_2]$	23[e]	34 ± 10[e]	0.0029 ± 0.0012	0.034 ± 0.008
$[Mn^{II}(Ris)_2]$	35[e]	14 ± 4[e]	0.0027 ± 0.0014	0.037 ± 0.004

[a] PGI: Percentage of growth inhibition of *T. cruzi* epimastigotes at 50 μM concentration of the compounds. [b] Concentration of compounds inhibiting 50% growth of *T. cruzi* amastigotes. [c] Concentration of compounds inhibiting 50% activity of *Tc*FPPS. [d] Concentration of compounds inhibiting 50% activity of *Hs*FPPS. [e] [37]

EXPGUI-GSAS suite.[54,55] Fig. S1 (ESI†) shows the final results for $C_{16}H_{52}Cu_2N_4O_{30}P_8\cdot 2H_2O$ compound, in the monoclinic $P2_1/c$ space group, confirming the crystalline structure of the series.

It is worth noting that the NiAle sample contains an unidentified impurity; the removal of the associated peaks in the indexing routine allows us to obtain the solution presented in Table 5.

In conclusion the X-ray powder diffraction data allow us to conclude that all obtained alendronate complexes are isostructural.

3.5 *In vitro* anti-*T. cruzi* activity

Growth inhibition of the epimastigote form of *T. cruzi* was studied in order to obtain a preliminary screening of the potential activity of the obtained complexes. The results are shown in Table 6. All metal complexes were more active against this form of the parasite than the corresponding alendronate and pamidronate ligands at 50 μM. Based on these results, complexes were assayed against intracellular amastigote forms of *T. cruzi*. The concentrations of complexes that inhibit 50% of the intracellular parasite growth (IC_{50} values) are shown in Table 6. All of them were potent growth inhibitors of the amastigote form of *T. cruzi* having IC_{50} values in the micromolar range. Similar results had been previously reported for metal–risedronate complexes (Table 6).[37] Pamidronate metal complexes showed quite similar activity – up to 4 fold more active than the free ligands. In addition, MPam complexes were not toxic to the mammalian Vero cells in all the assayed conditions (up to 50 μM) what could lead to good selectivity indexes. For alendronate complexes, results also showed an improvement of the anti-*T. cruzi* activity as a consequence of metal complexation. In this case, CuAle and MnAle were the most active compounds against amastigotes but selective indexes are not so favorable. For the risedronate and alendronate metal complexes, a clear dependence of the biological activity on the nature of the metal center could be observed, being manganese complexes the most active ones in both series and cobalt ones the less active. However, the effect of metal center in the pamidronate series seems to be much less pronounced.

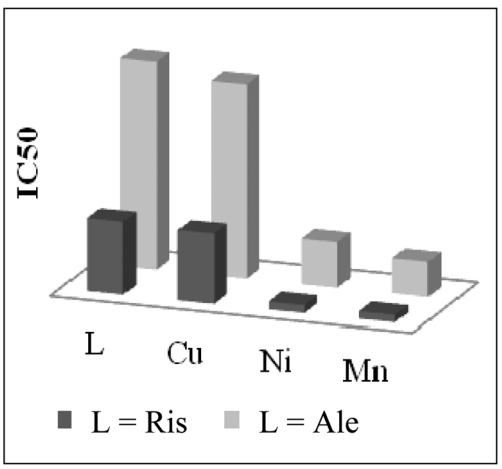

Fig. 5 Comparative inhibition of *Tc*PFFS by alendronate and risedronate metal complexes. IC_{50} values were scaled for clarity.

3.6 FPPS inhibition assays

The ability of the complexes to inhibit both *Tc*FPPS and *Hs*FPPS was assayed, as well as that of risedronate metal complexes previously obtained.[37] Results are depicted in Table 6. All complexes were better inhibitors of *Tc*FPPS than the corresponding ligands and IC_{50} values were, in most cases, 10 to 40 times lower for the complexes than for the free bisphosphonates. It has been stated that magnesium ions are necessary for the binding of bisphosphonates to FPPS.[11] Metal(II) ions present in the complexes could be responsible for an improved binding ability and hence a better activity. The most pronounced differences were observed for the series of alendronate complexes. Inhibition of *Tc*FPPS also seems to have a similar dependence on the metal nature for both risedronate and alendronate metal complexes (Fig. 5). For both series, cobalt complexes do not inhibit the

enzyme activity and manganese ones are the most active. As observed for the anti-*T. cruzi* activity, *Tc*FPPS inhibition values for the pamidronate complexes series did not show such significant variations. Additionally, a fairly good correlation could also be found between the ability of the complexes of inhibiting intracellular *T. cruzi* amastigote growth and *Tc*FPPS activity.

All complexes were also assayed on their ability for inhibiting *Hs*FPPS (Table 6). Alendronate and pamidronate complexes do not inhibit the activity of *Hs*FPPS in the assayed doses showing selectivity indexes of more than 100 in some cases. Risedronate metal complexes do inhibit *Hs*FPPS but inhibition values were 10 times higher than those of *Tc*FPPS. These results clearly evidenced that obtained metal complexes are selective inhibitors of *Tc*FPPS.

3.7 Interaction with proteins

The ability of alendronate and pamidronate metal complexes to interact with BSA was preliminary studied. Results are shown in Table S4 (ESI†). Interaction of a drug with plasma proteins could play a significant role in determining its bioavailability. For instance, plasma proteins might transport them to the corresponding target and several examples are reported in the literature, including drugs being currently evaluated in clinical trials.[56,57] Results show, in most cases, very high levels of BSA binding (from 52 to 98%) in the assayed conditions. These high levels of protein binding could eventually favor a complex's biological activity *in vivo* by overcoming their low solubility in aqueous solution as plasma proteins might transport them to the corresponding target.

4 Conclusions

Eight metal complexes with the bioactive bisphosphonates alendronate and pamidronate as ligands were synthesized. Complexes of the formula $[M_2^{II}(Ale)_4(H_2O)_2]\cdot 2H_2O$, with M = Cu, Co, Mn, Ni, and $([CuPam]\cdot H_2O)_n$ as well as $[M^{II}(Pam)_2(H_2O)_2]\cdot 3H_2O$ with M = Co, Mn and Ni were obtained and fully characterized. Most complexes are potent inhibitors of the intracellular amastigote form of *T. cruzi* and the ligands' activity increased as a consequence of metal complexation. The main mechanism of antiparasitic action of bisphosphonates, the inhibition of *Tc*FPPS, remains in the obtained metal complexes and an increase of enzyme levels of inhibition is also observed upon coordination. A fairly good correlation between the anti-*T. cruzi* activity and the *Tc*FPPS inhibition was observed. These complexes, as well as the previously obtained metal–risedronate ones, were demonstrated to be selective inhibitors of *Tc*FPPS showing no or little *Hs*FPPS inhibition. As expected, metal ions bind bisphosphonates through the ionizable phosphonate groups leading to neutral species. This fact, as well the possibility of proteins to transport the complexes in the blood could favor their bioavailability making them good candidates for further *in vivo* studies.

Acknowledgements

The authors wish to thank CSIC for financial support (CSIC project 352). B. D. thanks ANII for postgraduate scholarship. We thank K. Kavanagh and U. Oppermann for providing the human FPPS expression system and U.S. National Science Foundation (grant 0521237) for the X-ray diffractometer. Work in R. D. laboratory was funded by U.S. National Institutes of Health grant AI-82542. This work was performed under the auspices of RIDIMEDCHAG (CYTED) network.

References

1 A. Rassi Jr, A. Rassi and J. A. Marin-Neto, *Lancet*, 2010, **375**, 1388–1402.
2 G. A. Schmunis and Z. E. Yadon, *Acta Trop.*, 2010, **115**, 14–21.
3 G. Le Loup, G. Pialoux and F. X. Lescure, *Curr. Opin. Infect. Dis.*, 2011, **24**, 428–434.
4 A. Merlino, M. Gonzalez and H. Cerecetto, *Curr. Enzyme Inhib.*, 2010, **6**, 195–210.
5 J. A. Urbina, *Acta Trop.*, 2010, **115**, 55–68.
6 G. Rivera, V. Bocanegra-García, C. Ordaz-Pichardo, B. Nogueda-Torres and A. Monge, *Curr. Med. Chem.*, 2009, **16**, 3286–3293.
7 A. Montalvetti, B. N. Bailey, M. B. Martin, G. W. Severin, E. Oldfield and R. Docampo, *J. Biol. Chem.*, 2001, **276**, 33930–33937.
8 E. Oldfield, *Acc. Chem. Res.*, 2010, **43**, 1216–1226.
9 A. Mucha, P. Kafarski and Y. Berlicki, *J. Med. Chem.*, 2011, **54**, 5955–5980.
10 J. E. Dunford, A. A. Kwaasi, M. J. Rogers, B. L. Barnett, F. H. Ebetino, R. G. G. Russell, U. Oppermann and K. L. Kavanagh, *J. Med. Chem.*, 2008, **51**, 2187–2195.
11 M. J. Rogers, J. C. Crockett, F. P. Coxon and J. Mönkkönen, *Bone*, 2011, **49**, 34–41.
12 D. J. Hosfield, Y. Zhang, D. R. Dougan, A. Broun, L. W. Tari, R. V. Swanson and J. Finn, *J. Biol. Chem.*, 2004, **279**, 8526–8529.
13 K. L. Kavanagh, K. Guo, J. E. Dunford, X. Wu, S. Knapp, F. H. Ebetino, M. J. Rogers, R. G. R. Russell and U. Opperman, *Proc. Natl. Acad. Sci. U. S. A.*, 2006, **20**, 7829–7834.
14 J. M. Rondeau, F. Bitsch, E. Bourgier, M. Geiser, R. Hemmig, M. Kroemer, S. Lehmann, S. Rieffel, A. Strauss, J. R. Green and W. Jahnke, *ChemMedChem*, 2006, **1**, 267–273.
15 S. B. Gabelli, J. S. McLellan, A. Montalvetti, E. Oldfield, R. Docampo and L. M. Amzel, *Proteins: Struct., Funct., Bioinf.*, 2006, **62**, 80–88.
16 R. Docampo and S. N. J. Moreno, *Curr. Pharm. Des.*, 2008, **14**, 882–888.
17 J. A. Urbina, B. Moreno, S. Vierkotter, E. Oldfield, G. Payares, C. Sanoja, B. N. Bailey, W. Yan, D. A. Scott, S. N. J. Moreno and R. Docampo, *J. Biol. Chem.*, 1999, **274**, 33609–33615.
18 R. Docampo and S. N. J. Moreno, *Curr. Drug Targ.*, 2001, **1**, 51–61.
19 J. A. Urbina and R. Docampo, *Trends Parasitol.*, 2003, **19**, 495–501.
20 P. Vachal, J. J. Hale, Z. Lu, E. C. Streckfuss, S. G. Mills, M. MacCoss, D. H. Yin, K. Algayer, K. Manser, F. Kesisoglou, S. Ghosh and L. L. Alani, *J. Med. Chem.*, 2006, **49**, 3060–3063.
21 T. W. Hambley, *Dalton Trans.*, 2007, 4929–4937.
22 R. A. Sánchez-Delgado and A. Anzellotti, *Mini-Rev. Med. Chem.*, 2004, **4**, 159–165.
23 M. Navarro, G. Gabbiani, L. Messori and D. Gambino, *Drug Discovery Today*, 2010, **15**, 1070–1077.
24 S. P. Fricker, R. M. Mosi, B. R. Cameron, I. Baird, Y. Zhu, V. Anastassov, J. Cox, P. S. Doyle, E. Hansell, G. Lau, J. Langille, M. Olsen, L. Qin, R. Skerlj, R. S. Y. Wong, Z. Santucci and J. H. McKerrow, *J. Inorg. Biochem.*, 2008, **102**, 1839–1845.
25 L. Otero, P. Noblía, D. Gambino, H. Cerecetto, M. González, R. Di Maio, J. Ellena and O. E. Piro, *Inorg. Chim. Acta*, 2003, **344**, 85–94.
26 E. Cabrera, H. Cerecetto, M. González, D. Gambino, P. Noblía, L. Otero, B. Parajón-Costa, A. Anzellotti, R. Sánchez-Delgado, A. Azqueta, A. López de Ceráin and A. Monge, *Eur. J. Med. Chem.*, 2004, **39**, 377–382.
27 L. Otero, G. Aguirre, L. Boiani, M. González, A. Denicola, C. Rigol, C. Olea-Azar, J. D. Maya, A. Morello, D. Gambino and H. Cerecetto, *Eur. J. Med. Chem.*, 2006, **41**, 1231–1239.
28 L. Otero, M. Vieites, L. Boiani, A. Denicola, C. Rigol, L. Opazo, C. Olea-Azar, J. D. Maya, A. Morello, R. L. Krauth-Siegel, O. E. Piro, E. Castellano, M. González, D. Gambino and H. Cerecetto, *J. Med. Chem.*, 2006, **49**, 3322–3331.
29 C. Urquiola, M. Vieites, G. Aguirre, A. Marín, B. Solano, G. Arrambide, M. L. Lavaggi, M. H. Torre, M. González, A. Monge, D. Gambino and H. Cerecetto, *Bioorg. Med. Chem.*, 2006, **14**, 5503–5509.

30 L. Otero, P. Smircich, M. Vieites, M. Ciganda, P. Cardoso Severino, H. Terenzi, H. Cerecetto, D. Gambino and B. Garat, *J. Inorg. Biochem.*, 2007, **101**, 74–79.
31 L. Otero, C. Folch, G. Barriga, C. Rigol, L. Opazo, M. Vieites, D. Gambino, H. Cerecetto, E. Norambuena and C. Olea-Azar, *Spectrochim. Acta, Part A*, 2008, **70**, 519–523.
32 M. Vieites, L. Otero, D. Santos, D. Gajardo, J. Toloza, R. Figueroa, E. Norambuena, C. Olea-Azar, G. Aguirre, H. Cerecetto, M. González, A. Morello, J. D. Maya, B. Garat and D. Gambino, *J. Inorg. Biochem.*, 2008, **102**, 1033–1043.
33 M. Vieites, P. Smircich, B. Parajón-Costa, J. Rodríguez, V. Galaz, C. Olea-Azar, L. Otero, G. Aguirre, H. Cerecetto, M. González, A. Gómez-Barrio, B. Garat and D. Gambino, *JBIC, J. Biol. Inorg. Chem.*, 2008, **13**, 723–735.
34 M. Vieites, L. Otero, D. Santos, C. Olea-Azar, E. Norambuena, G. Aguirre, H. Cerecetto, M. González, U. Kemmerling, A. Morello, J. D. Maya and D. Gambino, *J. Inorg. Biochem.*, 2009, **103**, 411–418.
35 J. Benítez, L. Guggeri, I. Tomaz, G. Arrambide, M. Navarro, J. Costa Pessoa, B. Garat and D. Gambino, *J. Inorg. Biochem.*, 2009, **103**, 609–616.
36 M. Vieites, P. Smircich, L. Guggeri, E. Marchán, A. Gómez-Barrio, M. Navarro, B. Garat and D. Gambino, *J. Inorg. Biochem.*, 2009, **103**, 1300–1306.
37 B. Demoro, F. Caruso, M. Rossi, D. Benítez, M. Gonzalez, H. Cerecetto, B. Parajón-Costa, J. Castiglioni, M. Gallizi, R. Docampo, L. Otero and D. Gambino, *J. Inorg. Biochem.*, 2010, **104**, 1252–1258.
38 B. Demoro, C. Sarniguet, R. Sánchez-Delgado, M. Rossi, D. Liebowitz, F. Caruso, C. Olea-Azar, V. Moreno, A. Medeiros, M. A. Comini, L. Otero and D. Gambino, *Dalton Trans.*, 2012, **41**, 1534.
39 V. Kubícek, J. Kotek, P. Hermann and I. Lukes, *Eur. J. Inorg. Chem.*, 2007, 333–344.
40 G. M. Sheldrick, *Acta Crystallogr., Sect. A: Found. Crystallogr.*, 2008, **64**, 112–122.
41 C. Dong, *J. Appl. Crystallogr.*, 1999, **32**, 838.
42 A. Boultif and D. Louer, *J. Appl. Crystallogr.*, 2004, **37**, 724–731.
43 L. Huang, A. Lee and J. A. Ellman, *J. Med. Chem.*, 2002, **45**, 676–684.
44 A. M. Canavaci, J. M. Bustamante, A. M. Padilla, C. M. Pereza Brandan, L. J. Simpson, D. Xu, C. L. Boehlke and R. L. Tarleton, *PLoS Neglected Trop. Dis.*, 2010, **4**, e740.
45 K. L. Kavanagh, K. Guo, J. E. Dunford, X. Wu, S. Knapp, F. H. Ebetino, M. J. Rogers, R. G. Russell and U. Oppermann, *Proc. Natl. Acad. Sci. U. S. A.*, 2006, **103**, 7829–7834.
46 H. C. Rilling, *Methods Enzymol.*, 1985, **110**, 145–152.
47 K. Ogura, T. Nishino, T. Shinka and S. Seto, *Methods Enzymol.*, 1985, **110**, 155–167.
48 L. Messori, P. Orioli, D. Vullo, E. Alessio and E. Iengo, *Eur. J. Biochem.*, 2000, **267**, 1206–1213.
49 M. Juribašić and L. Tušek-Božić, *J. Mol. Struct.*, 2009, **924–926**, 66–72.
50 S. P. Man, M. Motevalli, S. Gardiner, A. Sullivan and J. Wilson, *Polyhedron*, 2006, **25**, 1017–1032.
51 C. Dufau, M. Benramdane, Y. Leroux, D. El Manouni, A. Neuman, T. Prange, J.-P. Silvestre and H. Gillier, *Phosphorus, Sulfur Silicon Relat. Elem.*, 1995, **107**, 145–148.
52 Z-C. Zhang, S-S. Bao and L-M. Zheng, *Inorg. Chem. Commun.*, 2007, **10**, 1063.
53 H. M. Rietveld, *J. Appl. Crystallogr.*, 1969, **2**, 65–71.
54 A. C. Larson and R. B. Von Dreele, General Structure Analysis System (GSAS), Los Alamos National Laboratory Report LAUR 2000, 86–748..
55 B. H. Toby, EXPGUI, J. Appl. Crystallogr. 2001, **34**, 210–213.
56 G. Dolman, B. Deacon and and T. W. Hambley, *J. Inorg. Biochem.*, 2002, **88**, 260–267.
57 B. P. Espósito and R. Najjar, *Coord. Chem. Rev.*, 2002, **232**, 137–149.

